Table 2. Gene expression changes observed in the dam's liver at 3 HAT

Gene	Function	GenBank#	Fold change	*t*-test
Up-regulated				
Heat shock protein hsp40-3	Stress	AA891542	2.61	0.000
70 kd heat-shock-like protein	Stress	M11942	1.92	0.038
Thioredoxin-like (32kD)	Stress	AA891694	1.74	0.015
PRG1	Cell growth	X96437	3.49	0.045
RJG-9 gene for c-jun	Transcription	AI175959	120.21	0.021
RL/IF-1	Transcription	X63594	25.78	0.014
LIM protein FHL2 (Fhl2)	Transcription	AA891527	2.50	0.044
3CH134/CL100 PTPase (oxidative stress-inducible protein tyrosine phosphatase)	Signal transduction	S81478	11.50	0.018
MAP kinase kinase kinase 1 (MEKK1)	Signal transduction	U48596	2.59	0.001
p38 mitogen activated protein kinase	Signal transduction	AA924542	2.09	0.040
Extracellular signal-related kinase (ERK3)	Signal transduction	M64301	2.01	0.008
14-3-3 protein	Signal transduction	D30740	1.85	0.000
Soluble IL-1 receptor type I	Receptor	U14010	6.43	0.000
Interleukin-1 receptor type I	Receptor	M95578	5.18	0.018
Tumor necrosis factor receptor	Receptor	M63122	2.98	0.000
Macrophage inflammatory protein-1alpha	Inflammation	U22414	28.06	0.000
Down-regulated				
Glycerol 3-phosphate acyltransferase	Lipid metabolism	U36771	−6.62	0.008
Trihydroxycoprostanoyl-CoA Oxidase	Lipid metabolism	X95189	−2.43	0.002
Apolipoprotein A-I (apoA-I)	Lipid metabolism	M00001	−2.37	0.015
Hydroxysteroid dehydrogenase, 11 beta type 1 (Hsd11b1)	Lipid metabolism	AI105448	−2.02	0.002
Cytochrome P-450-LA-omega (lauric acid omega-hydroxylase)	Drug metabolizing enzyme	AA924267	−2.44	0.001
Cytochrome P450 IIA2 protein (CYP2A2)	Drug metabolizing enzyme	J04187	−1.55	0.005
GST Yc2	Drug metabolizing enzyme	AA945082	−1.69	0.030
rGSTK1-1 (glutahione S-transferase subunit 13)	Drug metabolizing enzyme	AI105137	−1.53	0.036
Insulin growth factor-binding protein	Cell growth	J04486	−1.89	0.006
CDK5 activator-binding protein C53	Cell growth	AA799745	−1.56	0.003
CyclinG-associated kinase	Cell growth	D38560	−1.55	0.033

individual data showed a good correlation with those of the microarray analysis.

Discussion

T-2 toxin induces apoptosis in the lymphoid tissues and intestine. T-2 toxin also has fetotoxicity. We previously reported the histopathological changes in pregnant rats, and the number of apoptotic cells was increased in the liver of dams, placenta and fetal liver at 24 and 48 h after the T-2 toxin treatment (Sehata et al., 2003). It is reported that apoptosis induction by T-2 toxin involved activation of caspase-3 and -9 (Nagase et al., 2001). Yang et al. (2000) reported that apoptosis induction by satratoxins and other trichothecenes might involve the MAPK pathway. However, these studies were in vitro studies and T-2 toxin-induced toxicity in pregnant animals was still unclear. We performed microarray analysis of the liver, placenta and fetal liver from pregnant rats at 24 h after the T-2 toxin treatment, and showed that apoptosis-, oxidative stress-, lipid metabolism- and other metabolism-related genes were detected in all these tissues, suggesting that these factors may be involved in the T-2 toxin-induced toxicity (Sehata et al., 2004). However, in general, it is considered that gene expression changes are early event in response to the exposure of chemicals. In the present study, we performed microarray analysis at an earlier time point of the liver, placenta and fetal liver from pregnant rats treated with T-2 toxin. We also performed real-time RT-PCR analysis in selected genes and we confirmed that both data showed a good correlation.

From the results of the microarray analysis, the expression of oxidative stress-related genes such as the *HSP40, heme oxygenase* and *MnSOD* genes in the liver, *thioredoxin reductase, HSP70* and *metallothionein-2* and

Table 3. Gene expression changes observed in the dam's liver at 6 HAT

Gene	Function	GenBank#	Fold change	*t*-test
Up-regulated				
Manganese-containing superoxide dismutase (MnSoD)	Stress	Y00497	10.00	0.009
Heme oxygenase	Stress	J02722	2.20	0.008
hsp86	Stress	AA819776	1.55	0.040
Similar to growth arrest and DNA-damage-inducible 45 alpha	Cell growth	AI070295	69.41	0.030
p21 protein (cip1)	Cell growth	L41275	18.44	0.041
Transformed mouse 3T3 cell double minute 2 (Mdm2)	Cell growth	AI639488	11.30	0.008
Nuclear factor kappa B p105 subunit	Cell growth	L26267	11.25	0.035
TGFB inducible early growth response (Tieg)	Cell growth	AI071299	8.22	0.020
Bcl2-like 13 (apoptosis facilitator)	Cell growth	AA892271	1.73	0.012
Bax-alpha	Cell growth	U59184	1.61	0.014
Cbp/p300-interacting transactivator with Glu/Asp-rich carboxy-terminal domain 2 (Cited2)	Transcription	AA900476	8.91	0.042
Heat shock transcription factor 1	Transcription	AI172097	3.18	0.005
Protein-tyrosine kinase (JAK2)	Signal transduction	U13396	6.62	0.004
Smad1 protein (Smad1)	Signal transduction	AF067727	3.65	0.004
ICE-like cysteine protease (Lice)	Signal transduction	U49930	3.27	0.025
Protein kinase (MUK)	Signal transduction	D49785	2.29	0.010
TANK-binding kinase 1	Signal transduction	AI639447	2.26	0.024
p38 mitogen activated protein kinase (Mapk14)	Signal transduction	AI171630	1.80	0.010
Alpha-2-macroglobulin	Inflammation	M22670	49.75	0.003
Tumor necrosis factor receptor superfamily 1b	Receptor	AA900380	4.97	0.012
CC chemokine receptor protein	Receptor	E13732	2.52	0.018
Down-regulated				
17-Beta hydroxysteroid dehydrogenase type 2	Lipid metabolism	X91234	−4.48	0.024
Cholesterol 7-alpha-hydroxylase	Lipid metabolism	J05460	−4.29	0.025
Acyl coenzyme A dehydrogenase medium chain	Lipid metabolism	J02791	−3.33	0.004
Carnitine octanoyltransferase	Lipid metabolism	U26033	−2.70	0.004
Apolipoprotein A-IV	Lipid metabolism	M00002	−2.19	0.001
Cytochrome P-450d	Drug metabolism	K03241	−4.57	0.003
Cytochrome P-450e	Drug metabolism	M13234	−3.76	0.001
Cytochrome P-450b (phenobarbital-inducible)	Drug metabolism	L00320	−2.75	0.029
Cytochrome P-450 IV A1 (CYP4A1)	Drug metabolism	M57718	−2.59	0.021
Liver UDP-glucuronosyltransferase, phenobarbital-inducible form	Drug metabolism	M13506	−2.62	0.019
Glutathione S-transferase Yc2 subunit	Drug metabolism	S72506	−2.18	0.029
Max interacting protein 1 (Mxi1)	Cell growth	AA893611	−2.72	0.001
Cyclin-dependent kinase 4 (cdk4)	Cell growth	L11007	−2.12	0.012
DNase gamma	Cell growth	U75689	−2.10	0.015
Cyclin D1	Cell growth	D14014	−1.93	0.001
Cell cycle progression related D123	Cell growth	U34843	−1.77	0.031

Table 4. Gene expression changes observed in the placenta at 3 HAT

Gene	Function	GenBank#	Fold change	*t*-test
Up-regulated				
Oxidation resistance 1 (Oxr1)	Stress	H33461	1.68	0.047
NADPH-dependent thioredoxin reductase (TRR1)	Stress	AA891286	1.52	0.014
Cytocentrin	Cell growth	U82623	2.12	0.013
RL/IF-1	Transcription	X63594	1.55	0.035
Similar to mitogen-activated protein kinase kinase kinase 1 (MAPK/ERK kinase kinase 1) (MEK kinase 1) (MEKK 1)	Signal transduction	AI102620	1.56	0.012
Down-regulated				
Decorin	Signal transduction	AI639233	−2.02	0.030

Table 5. Gene expression changes observed in the placenta at 12 HAT

Gene	Function	GenBank#	Fold change	*t*-test
Up-regulated				
Heat shock protein 70	Stress	Z27118	7.74	0.047
Metallothionein-2 and metallothionein-1	Stress	AI176456	1.64	0.000
Macrophage inflammatory protein-2 precursor	Inflammation	U45965	14.53	0.007
Interleukin 1-beta	Inflammation	M98820	2.92	0.006
Nerve growth factor induced factor A	Cell growth	AF023087	13.27	0.026
Mdm2	Cell growth	AI639488	2.86	0.031
GADD45	Cell growth	L32591	2.21	0.045
P21 (c-Ki-ras)	Cell growth	U09793	1.56	0.019
v-Jun sarcoma virus 17 oncogene homolog (avian) (Jun)	Transcription	AA945867	2.94	0.017
RJG-9 gene for c-jun	Transcription	AI175959	2.83	0.004
RL/IF-1	Transcription	X63594	2.25	0.005
Nuclear factor kappa B p105 subunit	Transcription	L26267	2.20	0.000
c-Jun oncogene mRNA for transcription factor AP-1	Transcription	X17163	2.08	0.022
Cbp/p300-interacting transactivator with Glu/Asp-rich carboxy-terminal domain 2 (Cited2)	Transcription	AA900476	1.80	0.003
Protein-tyrosine phosphatase	Signal transduction	X58828	2.06	0.008
3CH134/CL100 PTPase (oxidative stress-inducible protein tyrosine phosphatase)	Signal transduction	S81478	1.69	0.035
Down-regulated				
Squalene epoxidase	Lipid metabolism	D37920	−2.60	0.008
7-Dehydrocholesterol reductase	Lipid metabolism	AB016800	−2.34	0.016
Glutathione S-transferase (GST) Y(b) subunit	Drug metabolizing enzyme	X04229	−1.97	0.003
Insulin-like growth factor-binding protein (IGF-BP3)	Cell growth	M31837	−2.16	0.003
Cyclin-dependent kinase 4 (cdk4)	Cell growth	L11007	−2.07	0.013
Cyclin D3	Cell growth	D16309	−1.98	0.004
Cyclin D1	Cell growth	D14014	−1.52	0.007
MASH-2	Transcription	X53724	−2.28	0.013
p38 Mitogen activated protein kinase	Signal transduction	U73142	−1.96	0.015
Similar to mitogen activated protein kinase kinase kinase kinase 1	Signal transduction	AA891302	−1.52	0.040
LDL-receptor	Receptor	X13722	−2.27	0.010
Pregnancy-specific beta 1-glycoprotein	Cell adhesion	U66292	−3.63	0.009
Spongiotrophoblast specific protein	Cell adhesion	AB009890	−3.11	0.025
Carcinoembryonic antigen-related protein	Cell adhesion	L00686	−2.78	0.004

Table 6. Gene expression changes observed in the fetal liver at 3 HAT (reference data)

Genes	Function	GenBank#	Fold change
Up-regulated			
CC chemokine ST38 precursor	Inflammation	AF053312	2.20
Mob-1	Inflammation	U17035	1.58
Interferon-gamma inducing factor isoform alpha precursor (IGIF)	Inflammation	U77777	1.52
Krox20	Transcription	U78102	1.60
Pregnancy-specific glycoprotein (rnCGM3)	Cell adhesion	U09815	1.89
Vascular cell adhesion molecule-1	Cell adhesion	M84488	1.54
Down-regulated			
Oxidosqualene lanosterol-cyclase	Lipid metabolism	E12275	−2.08
Acyl-CoA hydrolase	Lipid metabolism	AB010428	−2.00
Cytochrome P450 arachidonic acid epoxygenase (cyp 2C23)	Drug metabolism	U04733	−1.56
Glutathione s-transferase M5	Drug metabolism	U86635	−1.61
Growth arrest and DNA-damage-inducible protein GADD153	Cell growth	U30186	−3.13
Glioma-derived vascular endothelial cell growth factor	Cell growth	M32167	−1.52
Insulin-like growth factor I	Cell growth	M81183	−1.52
Caspase 6 (Mch2)	Signal transduction	AF025670	−1.54

Table 7. Gene expression changes observed in the fetal liver at 12 HAT

Gene	Function	GenBank#	Fold change	t-test
Up-regulated				
Metallothionein-2 and metallothionein-1	Stress	AI176456	9.37	0.000
Adrenomedullin precursor	Cell growth	D15069	4.37	0.039
Vascular endothelial growth factor A (VEGFA)	Cell growth	AA850734	2.88	0.003
MGADD45	Cell growth	L32591	2.30	0.009
Bax	Cell growth	S76511	1.73	0.034
Bax-alpha	Cell growth	U59184	1.51	0.031
Programmed cell death repressor BCL-X-Long	Cell growth	U34963	1.69	0.034
Mud-4	Cell growth	U70270	1.64	0.019
Gas-5 growth arrest homolog non-translated mRNA sequence	Cell growth	U77829	1.55	0.023
RJG-9 gene for c-jun	Transcription	AI175959	3.12	0.002
Cbp/p300-interacting transactivator with	Transcription	AA900476	2.19	0.004
Glu/Asp-rich carboxy-terminal domain 2 (Cited2) c-Fos	Transcription	X06769	2.02	0.019
Down-regulated				
Mitochondrial 3-hydroxy-3-methylglutaryl-CoA synthase	Lipid metabolism	M33648	−6.95	0.002
3-Hydroxy-3-methylglutaryl-Coenzyme A synthase 1 (Hmgcsl)	Lipid metabolism	AI177004	−3.13	0.024
17-Beta hydroxysteroid dehydrogenase type 2	Lipid metabolism	X91234	−4.02	0.025
Farnesyl diphosphate synthase (Fdps)	Lipid metabolism	AI180442	−3.64	0.014
Glutathione S-transferase Yc2 subunit	Drug metabolizing enzyme	S72506	−4.39	0.026
GST Yc2	Drug metabolizing enzyme	AA945082	−3.52	0.005
Cytochrome P-450-LA-omega (lauric acid omega-hydroxylase)	Drug metabolizing enzyme	AA997806	−3.04	0.026
Cyp4a locus encoding cytochrome P450 (IVA3)	Drug metabolizing enzyme	M33936	−2.98	0.023
Cytochrome P-450	Drug metabolizing enzyme	D13912	−2.55	0.006
Cyclin Dl	Cell growth	D14014	−2.12	0.005
Cyclin E	Cell growth	D14015	−1.52	0.011
p38 Mitogen activated protein kinase	Signal transduction	U73142	−2.46	0.002
p38 Mitogen activated protein kinase (Mapkl4)	Signal transduction	AI171630	−1.79	0.006
ICE-like cysteine protease (Lice)	Signal transduction	U49930	−2.04	0.017
MEK5alpha-l (MEK5)	Signal transduction	U37462	−1.75	0.018
14-3-3 Protein theta-subtype	Signal transduction	D17614	−1.70	0.024
Programmed cell death 8 (apoptosis-inducing factor)	Signal transduction	AA891591	−1.53	0.014

-1 in the placenta, and *metallothionein-2* and *-1* in the fetal liver increased. The real-time RT-PCR also confirmed the increased expression of *HSP70* in the placenta and the increased expression of *heme oxygenase* in the liver of dams. It is known that oxidative stress evokes various cellular events including apoptosis, growth arrest and activation of transcription factors. Oxidative stress causes lipid peroxidation and induces mitochondrial dysfunction. Mitocondrial dysfunction causes fatty acid β-oxidation and induces fatty liver (Jaeschke et al., 2002). T-2 toxin enhances lipid peroxidation (Chang and Mar, 1998). In addition, fatty liver was observed in the liver in our previous study (Sehata et al., 2003). The microarray results in the present study showed that the decreased expression of lipid metabolism-related genes suggested that the disturbance of lipid metabolism caused by oxidative stress occurred in the dam's liver, placenta and fetal liver by T-2 toxin.

Increased apoptosis in the liver of dams, placenta and fetal liver was observed histopathologically in this study. The expression of apoptosis-related genes such as the *GADD45, p21, cyclin D1, NF-kappa B, Bax-alpha, mdm2, c-jun, MEKK1, p38 MAPK* and *ERK3* genes, was changed by T-2 toxin treatment. MAPKs are important intermediates in signaling pathways for responding to extracellular stress. MAPKs play a role in cell growth, differentiation and apoptosis. For example, ERK mediates cell growth and protects cells from apoptosis, whereas JNK (c-Jun N-terminal kinase)

Table 8. Gene expression changes observed in the dam's liver, placenta and fetal liver

Gene	Function	GenBank#	Fold change				
			Liver		Placenta		Fetla liver
			3 HAT	6 HAT	3 HAT	12 HAT	12 HAT
All tissues							
Oxidation resistance 1 (Oxr1)	Stress	H33461		−1.87	1.68		−1.90
Protein disulfide isomerase-related protein (P5-pending)	Stress	AA892532		−1.81		−1.61	−1.59
Progression elevated gene 3 protein	Cell growth	AF020618	16.77			2.26	2.58
PRG1	Cell growth	X96437	3.49			2.13	1.70
Cyclin D1	Cell growth	D14014		−1.93		−1.52	−2.12
RJG-9 gene for c-jun	Transcription	AI175959	120.21			2.83	3.12
Cbp/p300-interacting transactivator with Glu/Asp-rich carboxy-terminal domain 2 (Cited2)	Transcription	AA900476		8.91		1.80	2.19
TIS 11	Immediate early gene	X63369	21.37			1.59	1.67
Initiation factor eIF-2B gamma subunit (eIF-2B gamma)	Translation	U38253		2.03		1.84	1.54
Protein tyrosine phosphatase	Signal transduction	U02553	8.45			1.97	3.45
p38 Mitogen activated protein kinase	Signal transduction	U73142	1.87			−1.96	−2.46
Glycoprotein processing glucosidase I	Metabolism	AF087431		−1.52		−1.73	−2.13
H2A and H2B histones	Cell structure	X59961		1.85		1.93	1.57
Liver and Placenta							
Transformed mouse 3T3 cell double minute 2 (Mdm2)	Cell growth	AI639488		11.30		2.86	
Nuclear factor kappa B p105 subunit	Cell growth	L26267		11.25		2.20	
Cyclin-dependent kinase 4 (cdk4)	Cell growth	L11007		−2.12		−2.07	
RL/IF-1	Transcription	X63594	25.78		1.55	2.25	
3CH134/CL100 PTPase	Signal transduction	S81478	11.50			1.69	
Glutathione S-transferase (GST) Y(b) subunit	Drug metabolism	X04229	1.55			−1.97	
Liver and Fetal liver							
Bax-alpha	Cell growth	U59184		1.61			1.51
p38 Mitogen activated protein kinase	Signal transduction	AA924542	2.09				−1.52
ICE-like cysteine protease (Lice)	Signal transduction	U49930		3.27			−2.04
17-Beta hydroxysteroid dehydrogenase type 2	Lipid metabolism	X91234		−4.48			−4.02
Cytochrome P-450	Drug metabolism	D13912		−2.34			−2.55
Glutathione S-transferase Yc2 subunit	Drug metabolism	S72506		−2.18			−4.39
Placenta and Fetal liver							
Metallothionein-2 and metallothionein-1	Stress	AI176456				1.64	9.37
GADD45	Cell growth	L32591				2.21	2.30
7-Dehydrocholesterol reductase	Lipid metabolism	AB016800				−2.34	−2.28

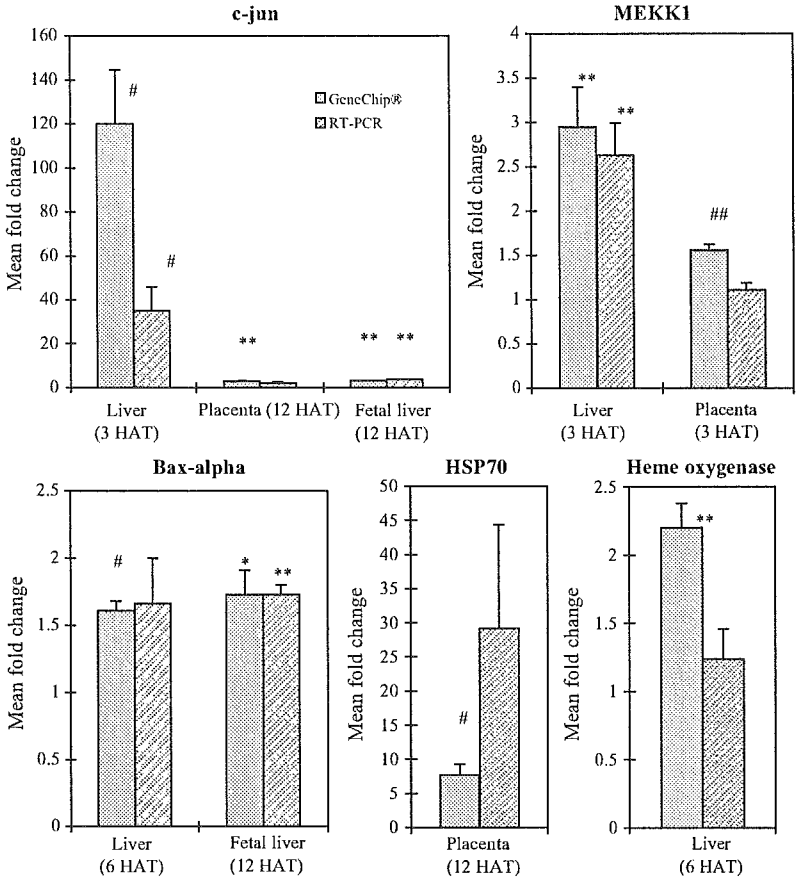

Fig. 3. Comparison of the fold changes in T-2 toxin-treated animals obtained from GeneChip® analysis and real-time RT-PCR analysis. The results of real-time RT-PCR (▨) showed a good correlation to that of GeneChip® analysis (□). Mean ± SE. Significantly different from control: $^{*}p<0.05$, $^{**}p<0.01$ (Student's *t*-test); $^{\#}p<0.05$, $^{\#\#}p<0.01$ (Welch's *t*-test).

and p38 MAPK inhibit cell proliferation and may promote apoptosis (Jarpe et al., 1998). Each MAPK is activated by an upstream MAPK kinase, including MEKK1, and activates transcription factors such as c-jun and c-fos. MEKK1 may induce apoptosis by causing a general deregulation of MAPK signaling (Boldt et al., 2003). In the present study, MAPK genes were detected by T-2 toxin treatment as described above. The real-time RT-PCR confirmed the increased expression of *MEKK1* gene. Increased expression of the *c-jun* gene was detected in all three tissues both in the microarray analysis and real-time RT-PCR analysis. c-Jun may also play a role in induction of apoptosis (Leppä and Bohmann, 1999). For example, negative regulation of NF-kappa B-dependent transcription of c-jun contributes to cisplatin-induced cell death (Sánchez-Pérez et al., 2002). NF-kappa B is generally involved in suppression of apoptosis by activating the expression of antiapoptotic genes (Kucharczak et al., 2003). However, NF-kappa B also plays a vital role in p53-mediated apoptosis (Ryan et al., 2000). Furthermore, NF-kappa B is a mediator of stress-induced gene expression. It is also known that MAPKs are involved in the NF-kappa B activation pathway (Mercurio and Manning, 1999). Therefore, the MAPK pathway may be involved in the mechanism of T-2 toxin-induced toxicity, and among many factors involved in this pathway, c-jun may play an important role in apoptosis induction (Fig. 4). In addition, increased expression of the *Bax-alpha* gene was detected in both liver and fetal liver. The real-time RT-PCR also confirmed the increased expression of the *Bax-alpha* gene in the liver and fetal liver. Bax is a member of the bcl-2 family and induces apoptosis. It is also reported that apoptosis induction in HL60 cells by T-2 toxin involved activation of caspase-3 and -9 through the release of cytochrome c from mitochondria in the cytosol (Nagase et al., 2001). Therefore, at least in the hepatic tissues, the Bax and caspase pathways may be involved in the mechanism of T-2 toxin-induced toxicity. On the other hand, increased expression of the *GADD45* and *p21* genes, and decreased expression of the *cyclin D1* gene were observed. This suggested that growth arrest or cell repair also occurred at the same time.

It is reported that the expression of phase I and II enzyme genes was decreased by T-2 toxin (Galtier et al., 1989; Guerre et al., 2000). We reported that decreased

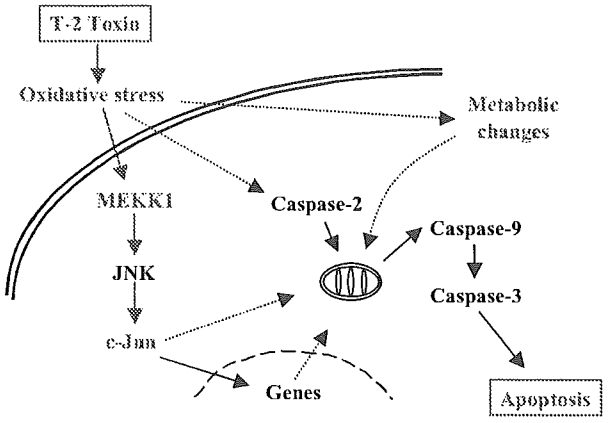

Fig. 4. Speculated mechanisms of T-2 toxin-induced toxicity in pregnant rats.

expression of drug-metabolizing enzyme genes was observed in the liver, placenta and fetal liver of pregnant rats at 24 HAT (Sehata et al., 2004). In the present study, decreased expression of drug-metabolizing enzyme genes was also observed in these tissues, indicating that this suppressive effect by T-2 toxin was a relatively early event.

When compared the differences in gene expression profiles in these tissues, the number of metabolism-related genes in the placenta was smaller than those in the dam's liver and fetal liver. This suggests that the placenta might play a less role in T-2 toxin metabolism. It is known that the expression of P450 genes in the fetal liver is different in the gestational days. The differences in the expression of P450 genes in the dam's liver and fetal liver obtained in the present study might reflect the difference of the basic expression of P450 genes in these tissues. In the placenta, we detected the decreased expression of cell adhesion-related genes, pregnancy-specific beta 1-glycoprotein, spongiotrophoblast specific protein and carcinoembryonic antigen-related protein. These genes express specifically in the placenta. As we do not know whether this change may reflect the morphological changes (apoptosis in cytotrophoblasts) or not, and specific in the placenta, we should examine the relation of T-2 toxin-induced apoptosis and cell adhesion changes in the other tissues more detail.

In the present study, the expression of oxidative stress-, apoptosis-, lipid metabolism- and drug-metabolizing enzyme-related genes was changed in the liver, placenta and fetal liver from pregnant rats treated with T-2 toxin. As regarding apoptosis, the MAPK pathway may be involved in the mechanism of T-2 toxin-induced apoptosis. In addition, increased expression of the *c-jun* gene was consistently observed in these tissues, suggesting that c-jun may be a key factor. In conclusion, it is speculated that in the mechanism of T-2 toxin-induced toxicity in pregnant rats, T-2 toxin induces oxidative stress, following by activation of the MAPK pathway, finally inducing apoptosis (Fig. 4). And the *c-jun* gene may play an important role in the induction of apoptosis. Further detailed studies are necessary to clarify the mechanism of T-2 toxin-induced toxicity.

Acknowledgements

We thank Mrs. K. Hara for preparation of histopathological samples, and Mrs. K. Watanabe and Mrs. N. Niino for conducting the microarray and real-time RT-PCR analyses.

References

Boldt S, Weidle UH, Kolch W. The kinase domain of MEKK1 induces apoptosis by dysregulation of MAP kinase pathways. Exp Cell Res 2003;283:80–90.

Chang IM, Mar WC. Effect of T-2 toxin on lipid peroxidation in rats: elevation of conjugated diene formation. Toxicol Lett 1998;40:275–80.

Galtier P, Paulin F, Eeckhoutte C, et al. Comparative effects of T-2 toxin and diacetoxyscirpenol on drug metabolizing enzymes in rat tissues. Food Chem Toxicol 1989;27:215–20.

Guerre P, Eeckhoutte C, Burgat V, et al. The effects of T-2 toxin exposure on liver drug metabolizing enzymes in rabbit. Food Addit Contam 2000;17:1019–26.

Hayes MA, Schiefer FB. Comparative toxicity of dietary T-2 toxin in rats and mice. J Appl Toxicol 1982;2:207–12.

Hoerr FJ, Carlton WW, Yagen B. Mycotoxicosis caused by a single dose of T-2 toxin or diacetoxyscirpenol in broiler chickens. Vet Pathol 1981;18:652–64.

Ishigami N, Shinozuka J, Katayama K, et al. Apoptosis in the developing mouse embryos from T-2 toxin-inoculated dams. Histol Histopathol 1999;14:729–33.

Ishigami N, Shinozuka J, Katayama K, et al. Apoptosis in mouse fetuses from dams exposed to T-2 toxin at different days of gestation. Exp Toxicol Pathol 2001;52:493–501.

Jaeschke H, Gores GJ, Cederbaum AI, et al. Mechanisms of hepatotoxicity. Toxicol Sci 2002;65:166–76.

Jarpe MB, Widmann C, Knall C, et al. Anti-apoptotic versus pro-apoptotic signal transduction: checkpoints and stop signs along the road to death. Oncogene 1998;17:1475–82.

Kucharczak J, Simmons MJ, Fan Y, et al. To be, or not to be: NF-κB is the answer—role of Rel/NF-κB in the regulation of apoptosis. Oncogene 2003;22:8961–82.

Laferge-Frayssinet C, Chakor K, Lafont P, et al. Transplacental transfer of T2-toxin: pathological effect. J Environ Pathol Toxicol Oncol 1990;10:64–8.

Leppä S, Bohmann D. Diverse function of JNK signaling and c-Jun in stress response and apoptosis. Oncogene 1999;18:6158–62.

Lühe A, Hildebrand H, Bach U, et al. A new approach to studying ochratoxin A (OTA)-induced nephrotoxicity: expression profiling in vivo and in vitro employing cDNA microarrays. Toxicol Sci 2003;73:315–28.

Marasas WFO, Bamburg JR, Smalley EB, et al. Toxic effects on trout, rats, and mice of T-2 toxin produced by the

fungus *Fusarium tricinctum* (Cd.) Snyd. Et Hans. Toxicol Appl Pharmacol 1969;15:471–82.

Martin LJ, Morse JD, Anthony A. Quantitative cytophotometric analysis of brain neuronal RNA and protein changes in acute T-2 mycotoxin poisoned rats. Toxicon 1986;24:933–41.

Mercurio F, Manning AM. NF-κB as a primary regulator of the stress response. Oncogene 1999;18:6163–71.

Middlebrook JL, Leatherman DL. Binding of T-2 toxin to eukaryotic cell ribosomes. Biochem Pharmacol 1989;38: 3103–10.

Nagase M, Alam MM, Tsushima A, et al. Apoptosis induction by T-2 toxin: activation of caspase-9, caspase-3, and DFF-40/CAD through cytosolic release of cytochrome c in HL-60 cells. Biosci Biotech Biochem 2001;65:1741–7.

Pang VF, Lorenzana RM, Beasley VR, et al. Experimental T-2 toxicosis in swine. III. Morphologic changes following intravascular administration of T-2 toxin. Fundam Appl Toxicol 1987;8:298–309.

Rousseaux CG, Schiefer HB. Maternal toxicity, embryolethality and abnormal fetal development in CD-1 mice following one oral dose of T-2 toxin. J Appl Toxicol 1987;7:281–8.

Ryan KM, Ernst MK, Rice NR, et al. Role of NF-κB in p53-mediated programmed cell death. Nature 2000;404:892–7.

Sánchez-Pérez I, Benitah SA, Martínez-Gomariz M, et al. Cell stress and MEKK1-mediated c-Jun activation modulate NFκB activity and cell viability. Mol Biol Cell 2002;13:2933–45.

Sehata S, Teranishi M, Atsumi F, et al. T-2 toxin-induced morphological changes in pregnant rats. J Toxicol Pathol 2003;16:59–65.

Sehata S, Kiyosawa N, Sakuma K, et al. Gene expression profiles in pregnant rats treated with T-2 toxin. Exp Toxic Pathol 2004;55:357–66.

Shinozuka J, Suzuki M, Noguchi N, et al. T-2 toxin-induced apoptosis in hematopoietic tissues of mice. Toxicol Pathol 1998;26:674–81.

Stanford GK, Hood RD, Hayes AW. Effect of prenatal administration of T-2 toxin to mice. Res Commun Chem Pathol Pharmacol 1975;10:743–6.

Sugamata M, Hattori T, Ihara T, et al. Fine structural changes and apoptotic cell death by T-2 mycotoxin. J Toxicol Sci 1998;23(Suppl. II):148–54.

Thompson WL, Wannemacher Jr. RW. In vivo effects of T-2 mycotoxin on synthesis of proteins and DNA in rat tissues. Toxicol Appl Pharmacol 1990;105:483–91.

Wang J, Fitzpatrick DW, Wilson JR. Effects of the trichothecene mycotoxin T-2 toxin on neurotransmitters and metabolites in discrete areas of the rat brain. Food Chem Toxicol 1998;36:947–53.

World Health Organization (WHO). Selected mycotoxins: ochratoxins, trichothecenes, ergot. Environmental health criteria, vol. 105. Geneva: WHO; 1990.

Yang GH, Jarvis BB, Chung YJ, et al. Apoptosis induction by the satratoxins and other trichothecene mycotoxins: relationship to ERK, p38 MAPK, and SAPK/JNK activation. Toxicol Appl Pharmacol 2000;164:149–60.

Yang MCK, Ruan QG, Yang JJ, et al. A statistical method for flagging weak spots improves normalization and ratio estimates in microarrays. Physiol Genomics 2001;7:45–53.

Available online at www.sciencedirect.com

SCIENCE DIRECT®

Neurotoxicology and Teratology 26 (2004) 579–586

NEUROTOXICOLOGY AND TERATOLOGY

www.elsevier.com/locate/neutera

Involvement of p53 in 1-β-D-arabinofuranosylcytosine-induced rat fetal brain lesions

Hirofumi Yamauchi*, Kei-ichi Katayama, Masaki Ueno, Koji Uetsuka, Hiroyuki Nakayama, Kunio Doi

Department of Veterinary Pathology, Graduate School of Agricultural and Life Sciences, The University of Tokyo, 1-1-1 Yayoi, Bunkyo, 113-8657 Tokyo, Japan

Received 22 January 2004; received in revised form 26 March 2004; accepted 26 March 2004
Available online 18 May 2004

Abstract

1-β-D-Arabinofuranosylcytosine (Ara-C), a cytidine analogue cytotoxic to proliferating cells, has a teratogenic effect in the brain of experimental animals and causes neural cell apoptosis in vitro and in vivo. In the present study, pregnant rats were injected with Ara-C on Day 13 of gestation and the fetal brain was collected from 1 to 48 h after treatment. Histopathological examinations revealed marked induction of apoptotic cell death and decrease of mitosis in neuroepithelial cells in the brain of Ara-C-treated fetus, and these changes were most prominent from 9 to 12 h. Expression of p53 protein, which mediates apoptosis and cell cycle arrest after DNA damage, was elevated remarkably and peaked at 3 h. *p21*, a cyclin-dependent kinase inhibitor responsible for p53-mediated cell cycle arrest, showed intense overexpression in protein and mRNA levels following the increase of p53 protein. The mRNA expressions of other p53 transcriptional target genes, *bax*, *cyclinG1*, and *fas*, also significantly increased and peaked at around 9 h. In conclusion, prenatal treatment of Ara-C is thought to induce apoptosis and inhibition of cell proliferation mediated by *p53* and its target genes in the fetal brain.

Keywords: Apoptosis; Ara-C; Fetus; p53; Rat; Central nervous system

1. Introduction

1-β-D-Arabinofuranosylcytosine (Ara-C), a cytidine analogue, inhibits DNA synthesis and is cytotoxic to proliferating cells especially in the DNA synthetic phase of the cell cycle [11]. Therefore, it has been used as one of the most effective agents in the clinical treatment for myelogenous leukemia [4] and other hematologic malignancies. On the other hand, prenatal treatment of Ara-C has a teratogenic effect and causes malformations of the brain such as encephalocele, hydrocephalus, and microcephaly in rats [1,5,22,23]. We previously reported that an injection of Ara-C into pregnant rats induced increased apoptosis in the brain and other organs of fetuses, which would be related with the teratogenicity of Ara-C [26].

The *p53* tumor suppressor gene is involved in the regulation of apoptosis and cell cycle arrest after DNA damage, thereby preventing the propagation of damaged cells in a number of different paradigms [15]. p21, a downstream target of p53, is an inhibitor of cyclin-dependent kinases and responsible for the cell cycle arrest in cells sustaining DNA damage [7].

Neural cells in various culture models develop apoptosis by the treatment of Ara-C, and p53 plays the key role in these responses [9,10,27]. It is also demonstrated that transplacental exposure of Ara-C failed to induce neural precursor cell apoptosis in the fetal telencephalon of *p53*-deficient mouse [6]. However, there are only a few reports regarding the incidence of apoptosis in the fetal brain exposed to Ara-C in vivo, and little is known about the expressional or functional patterns of *p53* and other related genes that would be essential for the cellular response to the Ara-C treatment.

The aim of the present study is to explore the more detailed process of Ara-C-induced cytotoxic effects in the developing fetal brain and to reveal its mechanisms in relation to *p53*. For the purpose, we examined the sequential histopathological changes in the fetal brain obtained from pregnant rats treated with Ara-C on Day 13 of gestation (GD13). Moreover, we investigated the

* Corresponding author. Tel./fax: +81-3-5841-8185.
E-mail address: yamauchi-h@umin.ac.jp (H. Yamauchi).

0892-0362/$ – see front matter © 2004 Elsevier Inc. All rights reserved.
doi:10.1016/j.ntt.2004.03.010

temporal expression patterns of p53 and p21 protein by immunohistochemistry and of *p53* and its target genes mRNAs by reverse transcription and polymerase chain reaction (RT-PCR).

2. Methods

2.1. Animals and chemicals

Pregnant Slc:Wistar rats (plug day: Day 0 of gestation) were obtained from Japan SLC, Shizuoka, Japan. They were kept under controlled conditions (temperature, 23 ± 2 °C; relative humidity, 55 ± 5%) using an isolator caging system (Niki Shoji, Tokyo) and were fed commercial pellets (MF, Oriental Yeast, Tokyo, Japan) and water ad libitum. Ara-C (Sigma, St. Louis, MO) was dissolved in phosphate-buffered saline (PBS). The protocol of the present study has been approved by the Animal Care and Use Committee of Graduate School of Agricultural and Life Sciences, The University of Tokyo.

2.2. Treatments

Pregnant rats were injected intraperitoneally with 250 mg/kg of Ara-C on GD 13. At 1, 3, 6, 9, 12, 24, and 48 h after treatment, six dams each were exsanguinated by heart puncture under ether anesthesia, and the fetuses were collected by Caesarian section. As controls, six pregnant rats were injected intraperitoneally with PBS on GD13 and sacrificed at the same time point as Ara-C-treated groups. Of the six dams obtained at each time point, three were used for histopathological and immunohistochemical analysis and three for RT-PCR analysis.

2.3. Histopathology and immunohistochemistry

Collected fetuses were fixed in 10% neutral-buffered formalin. For histopathological examination, 4-μm paraffin sections were stained with hematoxylin and eosin (HE).

For immunohistochemical examination, paraffin sections (4 μm) were deparaffinized and immersed in 10 mM citrate buffer, pH 6.0, and heated for 15 min at 121 °C by autoclave. After washing in Tris-buffered saline (TBS), the sections were placed in 0.3% H_2O_2-containing methanol for 30 min to inactivate endogenous peroxidase. Then the sections were incubated in skimmed milk for 40 min at 37 °C to reduce nonspecific staining and successively incubated in the rabbit anti-p53 polyclonal antibody (Santa Cruz Biotechnology, Santa Cruz, CA) or mouse anti-p21 monoclonal antibody (PharMingen, San Diego, CA) overnight at 4 °C and then in EnVision+polymer reagent (Dako, Carpinteria, CA) for 30 min at room temperature. These sections were washed in TBS for 15 min after each step. The positive signals were visualized using a peroxidase–diaminobenzidine reaction and then the sections were counterstained with methylgreen.

2.4. Morphometry

Apoptotic and mitotic neuroepithelial cells in the ventricular zone of the fetal telencephalic wall were counted in two randomly chosen fetuses from a dam on the HE-stained sections under light microscope. Five hundred cells were counted in each fetus. p53- or p21-positive surviving neuroepithelial cells were also counted in the same way on the immunohistochemically stained sections under light microscope. The apoptotic, mitotic, and p53- or p21-labeling indices (%) were expressed as the mean ± S.D. for three dams, and statistical analysis was carried out with Student's *t* test.

2.5. RNA extraction and semiquantitative RT-PCR

Six fetal telencephalon from a dam were pooled and total RNA was extracted using Isogen (Nippon Gene, Toyama, Japan). The reverse transcriptase reaction for synthesis of the first strand cDNA was carried out with 15 μg of sample in 60 μl of reaction mixture using oligo(dT)$_{12-18}$ primer and a Superscript Preamplification System (Invitrogen, Carlsbad, CA). Polymerase chain reaction was performed with pairs of oligonucleotide primers corresponding to the cDNA sequences of rat mRNA (Table 1). PCR was carried out with 1 μl of RT product in a 100-μl reaction mixture containing 50 pM of sense and antisense primer, 1.25 U rTaq, 10 × PCR buffer, and dNTP mixture (Takara, Ohtsu, Japan). This was immediately followed by preheating at 94 °C for 7 min, denaturation at 94 °C for 1 min, annealing at 58.5 °C for

Table 1
Primer sequences and cycle numbers

Gene	Sense primer	Antisense primer	Cycle number
p53	ATATGAGCATCGAGCTCCCTCT	CACAACTGCACAGGGCATGT	25
p21	AAGTATGCCGTCGTCTGTTCG	GGCACTTCAGGGCTTTCTCTT	28
bax	TTCATCCAGGATCGAGCAGAG	TGAGGACTCCAGCCACAAAGAT	25
cyclinG1	GTGTCGGACTGAGCTGCTTTT	TTGGGAGGTGGGTTATCCTGT	24
fas	AAGAGGAGCGTTCGTGAAACC	GATCAGCAGCCAAAGGAGCTTA	30
GAPDH	GCTTCACCACCTTCTTGATGTC	GAGTATGTCGTGGAGTCTACTG	20

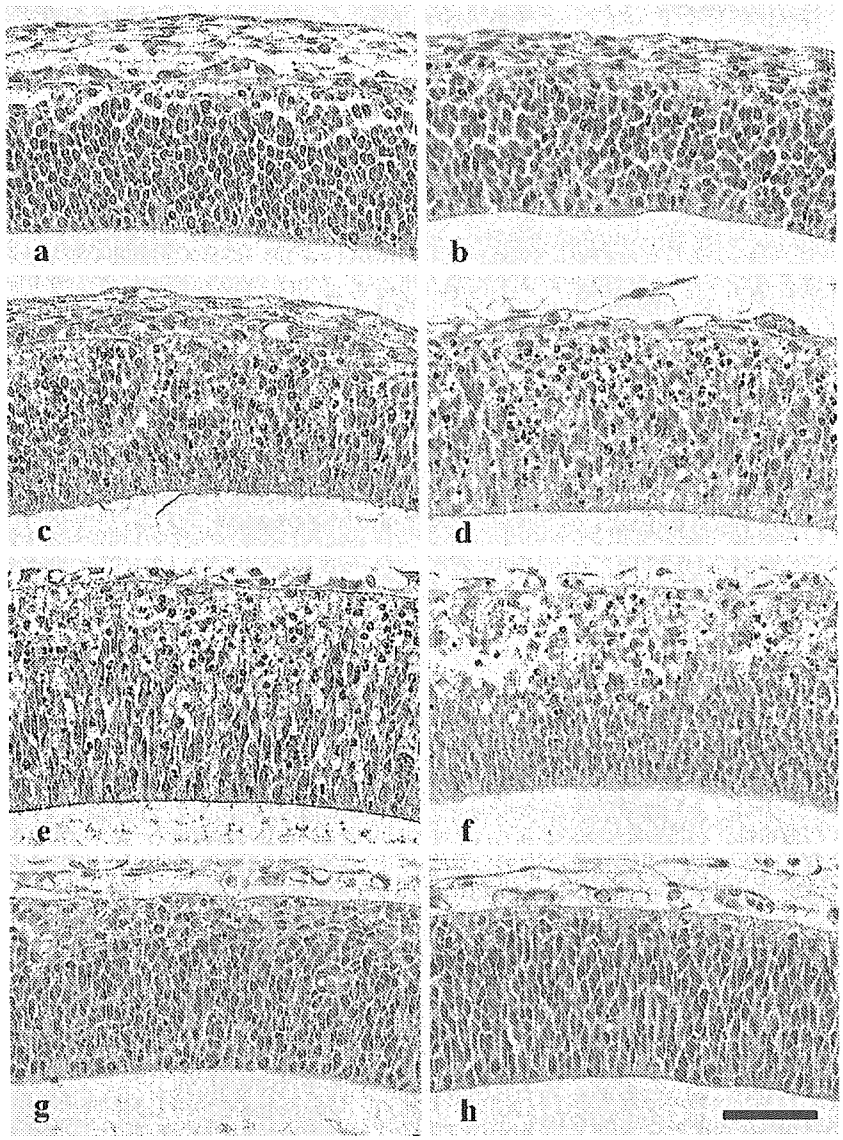

Fig. 1. Histological appearances of the telencephalic wall of the Ara-C-treated group at 1 (a), 3 (b), 6 (c), 9 (d), 12 (e), 24 (f), and 48 h (g) and of the control group at 9 h after treatment (h). Apoptotic cells were found from 3 h. The number of apoptotic cells peaked at 9 h, then gradually decreased and returned to the control level at 48 h. The number of mitotic cells decreased from 3 h and few mitotic cells were observed from 9 to 12 h. Then mitotic index began to recover from 24 h and reached the control level at 48 h. HE; Bar = 60 μm.

1 min, and extension at 72 °C for 1 min using Takara PCR Thermal Cycler MP (Takara). Cycle numbers for different PCR reactions are shown in Table 1. Optimal cycle numbers were determined by the preliminary experiment to ensure that the amplification of each gene was in the linear range and not during the plateau phase. PCR products were identified by electrophoresis on 2% agarose gels (Nippon Gene) followed by ethidium bromide (Invitrogen) staining. Fluorescent gel imaging was carried out using a UV-CCD video system Fas-III (Toyobo, Tokyo, Japan). The results are shown as a relative ratio to glyceraldehyde-3-phosphate dehydrogenase (GAPDH) expression. The relative band density is presented as the mean ± S.D. for three dams and statistical analysis was carried out using Student's *t* test.

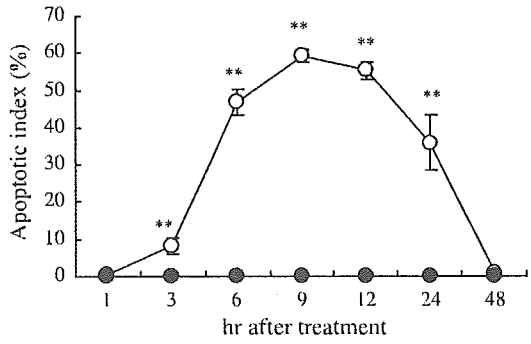

Fig. 2. Apoptotic index in the telencephalic wall of rat fetuses exposed to Ara-C on GD13. Data represent the mean ± S.D. ($n = 3$). $^{**}P < 0.01$; significantly different from controls. Open circles, Ara-C-treated group; closed circles, control group.

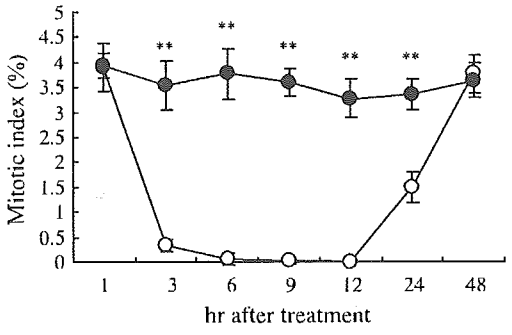

Fig. 3. Mitotic index in the telencephalic wall of rat fetuses exposed to Ara-C on GD13. Data represent the mean ± S.D. ($n=3$). $**P<0.01$; significantly different from controls. Open circles, Ara-C-treated group; closed circles, control group.

3. Results

3.1. Histopathology

After transplacental exposure of Ara-C, the number of pyknotic neuroepithelial cells, which were shown to be apoptotic ones in our previous study [26], significantly increased in the ventricular zone of the fetal brain. The number began to increase from 3 h and peaked from 9 to 12 h after treatment. It declined from 24 h and nearly returned to the control level at 48 h. Few apoptotic cells were observed in the fetal brain from control dams throughout the experimental period (Figs. 1 and 2).

In the Ara-C-treated group, the number of mitotic figures of neuroepithelial cells in the ventricular zone began to

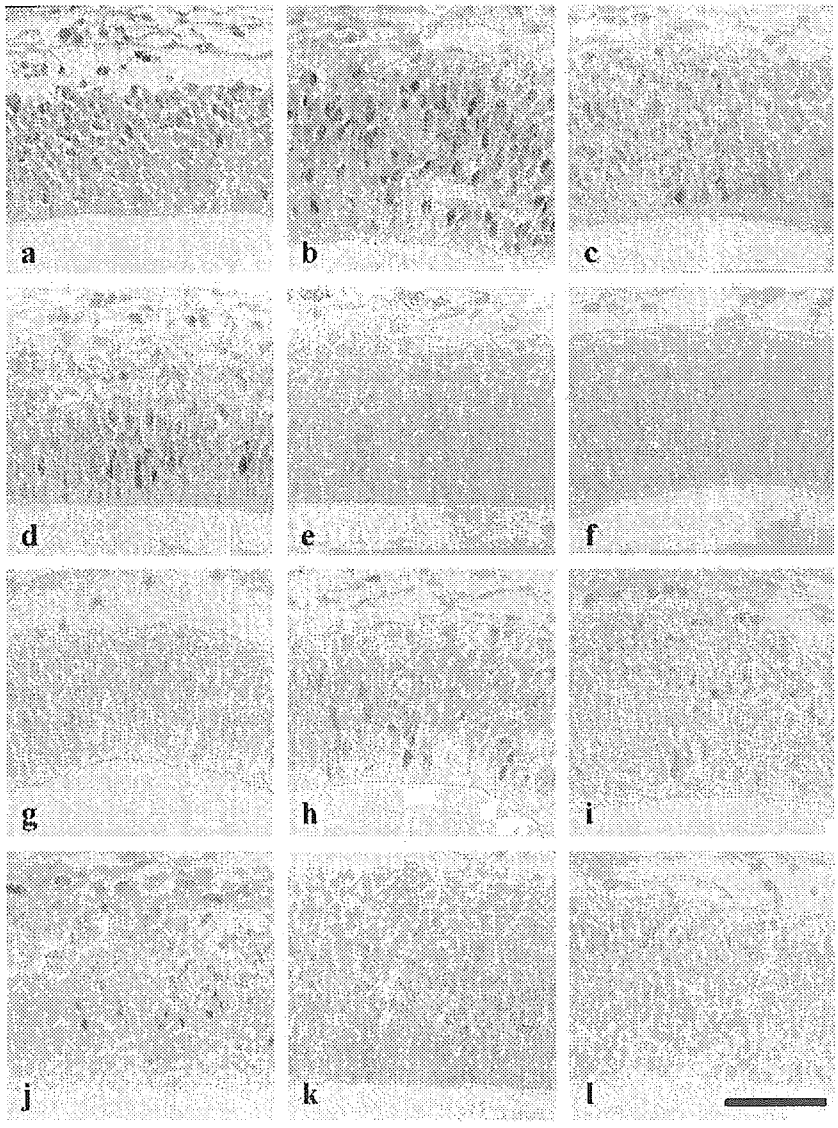

Fig. 4. Immunostaining for p53 (a–f) and p21 (g–l) in the telencephalic wall of rat fetuses. The number of p53-positive cells began to increase from 1 h (a) and reached the peak at 3 h after treatment (b). Then the number declined (c; 9 h) but increased again at 24 h (d). Finally, the number decreased and returned to the control level at 48 h (e). The number of p21-positive cells hardly changed until 3 h (g) and then abruptly peaked at 6 h (h). Subsequently, the number declined (i; 9 h) but again increased at 24 h (j). Finally, the number decreased and returned to the control level at 48 h (k). In the control fetuses, only a few p53- and p21-positive signals were observed (f and l). Bar = 60 μm.

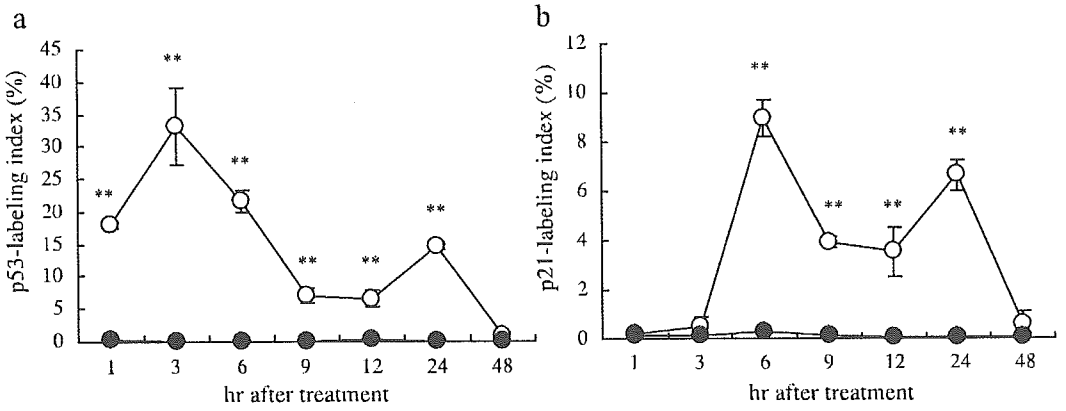

Fig. 5. p53 (a)- and p21-labeling index (b) in the telencephalic wall of rat fetuses exposed to Ara-C on GD13. Data represent the mean ± S.D. ($n=3$). ** $P<0.01$; significantly different from controls. Open circles, Ara-C-treated group; closed circles, control group.

decrease markedly from 3 h and few mitotic cells were observed from 9 to 12 h. Then the number began to recover from 24 h and reached the control level at 48 h. Mitotic index hardly changed in the control group throughout the experimental period (Figs. 1 and 3).

3.2. Immunohistochemistry

In the ventricular zone of the Ara-C-treated fetuses, the number of p53-positive signals in the nuclei of neuroepithelial cells increased from 1 h and peaked at 3 h after treatment. Then the number declined from 6 to 12 h but increased again at 24 h. Finally, the number decreased and returned to the control level at 48 h (Figs. 4a–e and 5a).

The number of p21-positive signals in the nuclei of neuroepithelial cells increased and reached the peak abruptly at 6 h. Then the number declined from 9 to 12 h and increased again at 24 h. Finally, the number decreased and returned to the control level at 48 h (Figs. 4g–k and 5b).

In the control fetuses, only a few p53- and p21-positive signals were observed in the nuclei of neuroepithelial cells throughout the experimental period (Figs. 4f, l, and 5).

3.3. Semiquantitative RT-PCR

The expressions of *p53* mRNA did not increase significantly throughout the experimental period. The expression of *p21*, *bax*, *cyclinG1*, and *fas* mRNAs significantly increased in the Ara-C-treated group. The expression of *p21* mRNA increased prominently from 3 to 24 h, and those of *bax*, *cyclinG1*, and *fas* mRNAs also increased and peaked at around 9 h after treatment (Figs. 6 and 7).

4. Discussion

p53 is activated by DNA-damaging agents or mitotic inhibitors [15]. It transactivates a series of genes including *p21* [8], *bax* [24], *cyclinG1* [20], and *fas* [19]. p21 is an inhibitor of cyclin-dependent kinases and it induces cell cycle arrest at G1 phase [7]. Bax is a proapoptotic member of the bcl-2 family. Increased bax/bcl-2 ratio enforces dimerization of *bax* and finally induces apoptosis [12]. CyclinG1 dephosphorylates mdm2, a negative regulator of p53, and modulates its function [21]. Fas is a type I membrane protein that belongs to tumor necrosis factor receptor/nerve growth factor receptor family [13] and it induces apoptosis when it binds to *fas* ligand.

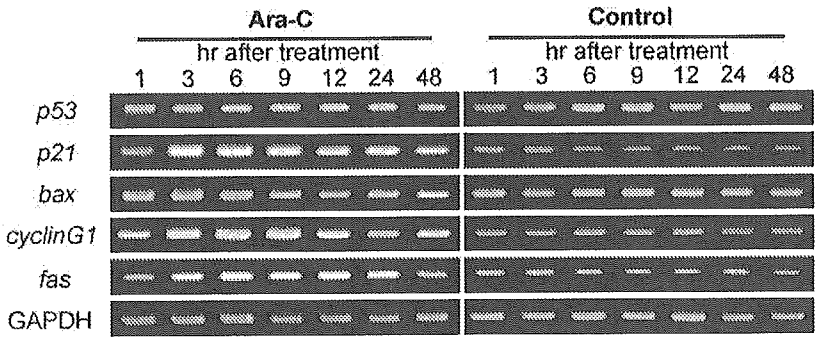

Fig. 6. Sequential changes of mRNA expression of p53 and its target genes. Agarose gel electrophoresis. Expressions of p53 target genes are elevated after Ara-C treatment.

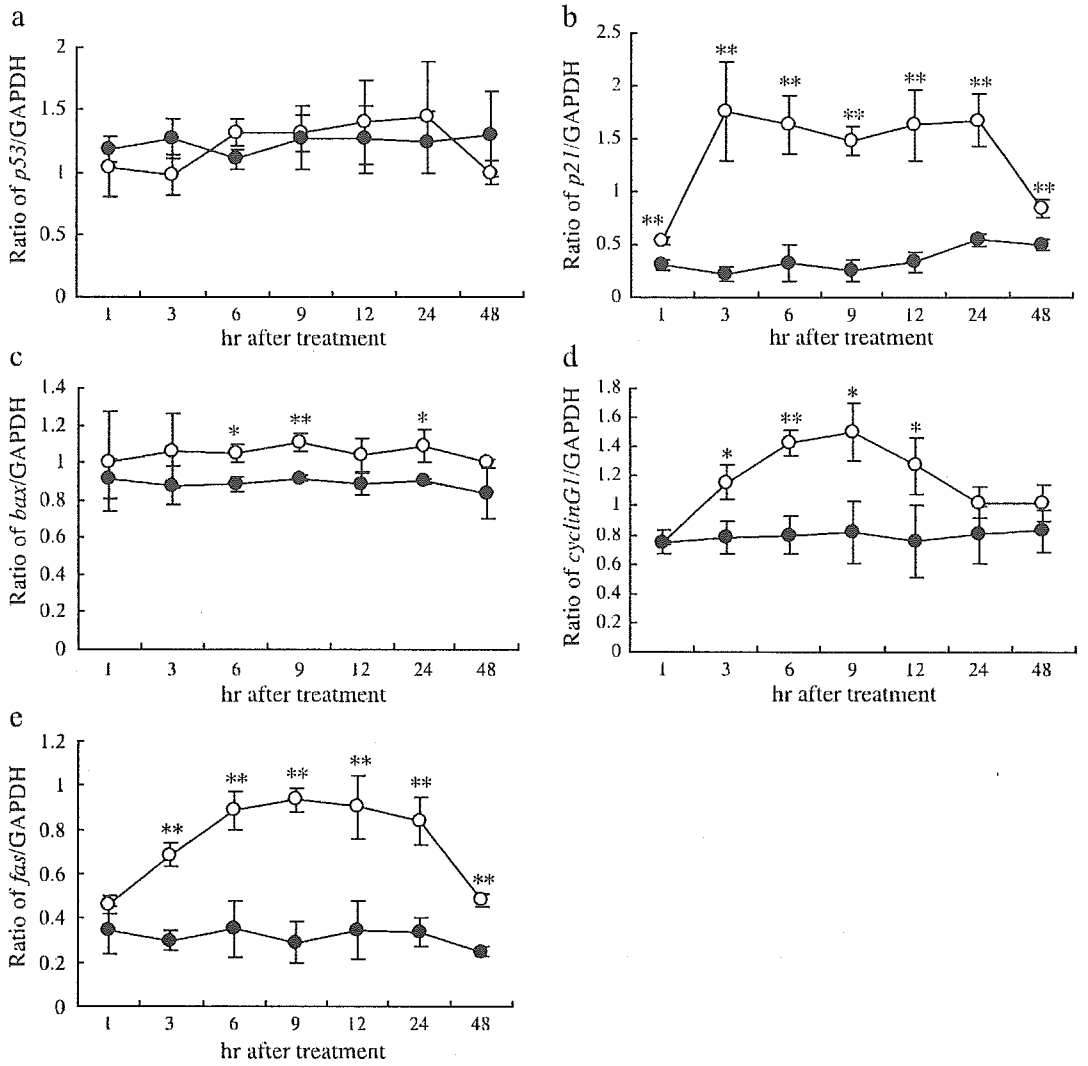

Fig. 7. Sequential changes of mRNA expression of *p53* (a), *p21* (b), *bax* (c), *cyclinG1* (d), and *fas* (e) in the brain of rat fetuses exposed to Ara-C on GD13. Data represent the mean ± S.D. ($n=3$). $*P<0.05$, $**P<0.01$; significantly different from controls. Open circles, Ara-C-treated group; closed circles, control group.

In the present study, the incidence of apoptosis in neuroepithelial cells of the fetal brain increased markedly whereas the number of mitotic cells decreased prominently after treatment with Ara-C. In addition, incorporation of 5-bromo-2′-deoxyuridine (BrdU) into neuroepithelial cell nuclei remarkably decreased after Ara-C treatment (data not shown). Immunohistochemical analysis revealed that the substantial increase of p53 protein expression preceded these histological changes. RT-PCR analysis showed that the expression of *p21* mRNA, which elevated most prominently among p53 target genes examined, began to increase markedly from 3 h after treatment when p53 protein level reached the peak. Subsequently, the expression of p21 protein increased and reached the maximal value at 6 h. The expressions of p53 and p21 protein increased again at 24 h and their expression patterns were well coincided with each other. The expression of other p53 target genes mRNAs significantly increased and peaked at around 9 h following the elevation of p53 protein. These findings suggest that accumulation of p53 protein transactivated its target genes including *p21* in the Ara-C-treated fetal brain. Since the mitotic index was suppressed during overexpression of p21, it is likely that p21 plays an important role in the induction of cell cycle arrest also in the present study. Neural precursor cells in the fetal telencephalon of *p53*-deficient mice did not develop apoptosis by the transplacental exposure of Ara-C [6], indicating that p53 is essential in Ara-C-induced apoptosis in vivo.

Our data suggest that transplacental exposure of Ara-C caused an induction of apoptosis and an inhibition of cell proliferation mediated by p53 and its transcriptional target genes in the fetal brain. On the other hand, though p21 is known to induce G1 arrest [7], it is not possible to confirm in which phase neuroepithelial cell cycle was arrested or retarded in our experiment, and further studies are needed to clarify this point.

In response to DNA damage, p53 protein is phosphorylated and becomes stabilized against disruption by the interaction with its negative regulator, mdm2. In a lot of cases, functional activation of p53 is mediated by the posttranscriptional mechanism increasing the half-life of the protein [16]. In our case, overexpression of *p53* mRNA was not detected in spite of the increase in p53 protein level, and this suggests that p53 is regulated by such a protein stabilization mechanism. In addition, immunohistochemical staining revealed that increased expression of p53 protein is localized in nuclei of neuroepithelial cells in the present study. This is consistent with the fact that p53 is accumulated and binds DNA in the nucleus of the damaged cell to exert its function [15].

Other DNA damaging teratogenic drugs, such as ethylnitrosourea and 5-azacytidine, also caused apoptosis and cell cycle arrest in the fetal brain with up-regulation and activation of p53 protein [14,25]. Besides chemicals, radiation induced apoptosis in the rat fetal brain in a *p53*-dependent manner [2], and brain anomalies were detected after birth [18]. These findings suggest that neural cells in the fetal brain are susceptible to DNA damaging stimuli, easily develop apoptosis and cell cycle arrest in a p53-dependent way, and a consequent decrease of neural cell population induced by excess cell death and suppressed cell proliferation may contribute to the formation of brain anomalies.

In the present study, secondary peaks were observed in the expression patterns of p53 and p21 protein at 24 h after treatment. Although further studies are needed to clarify its meaning, there are two possible explanations for this finding. First, neuroepithelial cells in the telencephalic ventricular zone are not composed of homogeneous cells; thus, reactions to Ara-C treatment would be different among those cells. In the stage of brain development, neuroepithelial cells move in the ventricular zone following a particular pattern [17]. In the process of their cell cycle, the nuclei of the neuroepithelial cells descend to the ventricular inner surface to undergo mitosis and subsequently return to the outer zone again. After that, some daughter cells move to cortical plate to differentiate into neuroblasts and others maintain their function as neuroepithelial cells and continue cell cycle in the ventricular zone. Thus, it is possible that protein expression patterns after Ara-C exposure were not the same in these cells even if they incorporate the drug at the same time, thereby resulting in the two separate peaks in the expression of p53 and p21 protein. Second, maternal and placental toxicity of Ara-C would affect the fetal tissues including brain. Prenatal treatment of Ara-C induced apoptosis in various fetal tissues such as hematopoietic progenitor cells and in placental trophoblasts [26]. Excess cell death in fetal tissues and placenta would impair the sustenance of brain development and indirectly increase p53 protein and its targets. Indeed, it is demonstrated that hypoxia caused p53 protein accumulation and overexpression of its downstream targets in cultured neuron [3].

In conclusion, our data suggest that transplacental exposure of Ara-C caused an induction of neuroepithelial cell apoptosis and an inhibition of cell proliferation through the mechanisms mediated by p53 and its transcriptional target genes in the fetal brain.

References

[1] B.P. Adlard, J. Dobbing, J. Sands, A comparison of the effects of cytosine arabinoside and adenine arabinoside on some aspects of brain growth and development in the rat, Br J Pharmacol 54 (1975) 33–39.

[2] S. Bolaris, E. Bozas, A. Benekou, H. Philippidis, F. Stylianopoulou, In utero radiation-induced apoptosis and p53 gene expression in the developing rat brain, Int J Radiat Biol 77 (2001) 71–81.

[3] C. Bossenmeyer-Pourie, V. Lievre, S. Grojean, V. Koziel, T. Pillot, J.L. Daval, Sequential expression patterns of apoptosis- and cell cycle-related proteins in neuronal response to severe or mild transient hypoxia, Neuroscience 114 (2002) 869–882.

[4] R.L. Capizzi, Curative chemotherapy for acute myeloid leukemia: the development of high-dose ara-C from the laboratory to bedside, Invest New Drugs 14 (1996) 249–256.

[5] S. Chaube, W. Kreis, K. Uchida, M.L. Murphy, The teratogenic effect of 1-β-D-arabinofuranosylcytosine in the rat. Protection by deoxycytidine, Biochem Pharmacol 17 (1968) 1213–1216.

[6] C. D'Sa-Eipper, J.R. Leonard, G. Putcha, T.S. Zheng, R.A. Flavell, P. Rakic, K. Kuida, K.A. Roth, DNA damage-induced neural precursor cell apoptosis requires p53 and caspase 9 but neither Bax nor caspase 3, Development 128 (2001) 137–146.

[7] V. Dulic, W.K. Kaufmann, S.J. Wilson, T.D. Tlsty, E. Lees, J.W. Harper, S.J. Elledge, S.I. Reed, p53-dependent inhibition of cyclin-dependent kinase activities in human fibroblasts during radiation-induced G1 arrest, Cell 76 (1994) 1013–1023.

[8] W.S. el-Deiry, T. Tokino, V.E. Velculescu, D.B. Levy, R. Parsons, J.M. Trent, D. Lin, W.E. Mercer, K.W. Kinzler, B. Vogelstein, WAF1, a potential mediator of p53 tumor suppression, Cell 75 (1993) 817–825.

[9] Y. Enokido, T. Araki, S. Aizawa, H. Hatanaka, p53 involves cytosine arabinoside-induced apoptosis in cultured cerebellar granule neurons, Neurosci Lett 203 (1996) 1–4.

[10] H.M. Geller, K.Y. Cheng, N.K. Goldsmith, A.A. Romero, A.L. Zhang, E.J. Morris, L. Grandison, Oxidative stress mediates neuronal DNA damage and apoptosis in response to cytosine arabinoside, J Neurochem 78 (2001) 265–275.

[11] S. Grant, Ara-C: cellular and molecular pharmacology, Adv Cancer Res 72 (1998) 197–233.

[12] A. Gross, J. Jockel, M.C. Wei, S.J. Korsmeyer, Enforced dimerization of BAX results in its translocation, mitochondrial dysfunction and apoptosis, EMBO J 17 (1998) 3878–3885.

[13] N. Itoh, S. Yonehara, A. Ishii, M. Yonehara, S. Mizushima, M. Sameshima, A. Hase, Y. Seto, S. Nagata, The polypeptide encoded by the cDNA for human cell surface antigen Fas can mediate apoptosis, Cell 66 (1991) 233–243.

[14] K. Katayama, R. Ohtsuka, H. Takai, H. Nakayama, K. Doi, Expression of p53 and its transcriptional target genes mRNAs in the ethylnitrosourea-induced apoptosis and cell cycle arrest in the fetal central nervous system, Histol Histopathol 17 (2002) 715–720.

[15] L.J. Ko, C. Prives, p53: puzzle and paradigm, Genes Dev 10 (1996) 1054–1072.

[16] N.D. Lakin, S.P. Jackson, Regulation of p53 in response to DNA damage, Oncogene 18 (1999) 7644–7655.

[17] J. Langman, R.L. Guerrant, B.G. Freeman, Behavior of neuro-epithelial cells during closure of the neural tube, J Comp Neurol 127 (1966) 399–411.

[18] T. Miki, Y. Fukui, Y. Takeuchi, M. Itoh, A quantitative study of the effects of prenatal X-irradiation on the development of cerebral cortex in rats, Neurosci Res 23 (1995) 241–247.

[19] M. Muller, S. Wilder, D. Bannasch, D. Israeli, K. Lehlbach, M. Li-Weber, S.L. Friedman, P.R. Galle, W. Stremmel, M. Oren, P.H. Krammer, p53 activates the CD95 (APO-1/Fas) gene in response to DNA damage by anticancer drugs, J Exp Med 188 (1998) 2033–2045.

[20] K. Okamoto, D. Beach, Cyclin G is a transcriptional target of the p53 tumor suppressor protein, EMBO J 13 (1994) 4816–4822.

[21] K. Okamoto, H. Li, M.R. Jensen, T. Zhang, Y. Taya, S.S. Thorgeirsson, C. Prives, Cyclin G recruits PP2A to dephosphorylate Mdm2, Mol Cell 9 (2002) 761–771.

[22] D.H. Percy, Teratogenic effects of the pyrimidine analogues 5-iododeoxyuridine and cytosine arabinoside in late fetal mice and rats, Teratology 11 (1975) 103–117.

[23] E.J. Ritter, W.J. Scott, J.G. Wilson, Teratogenesis and inhibition of DNA synthesis induced in rat embryos by cytosine arabinoside, Teratology 4 (1971) 7–13.

[24] M. Selvakumaran, H.K. Lin, T. Miyashita, H.G. Wang, S. Krajewski, J.C. Reed, B. Hoffman, D. Liebermann, Immediate early up-regulation of bax expression by p53 but not TGF beta 1: a paradigm for distinct apoptotic pathways, Oncogene 9 (1994) 1791–1798.

[25] M. Ueno, K. Katayama, H. Nakayama, K. Doi, Mechanisms of 5-azacytidine (5AzC)-induced toxicity in the rat foetal brain, Int J Exp Pathol 83 (2002) 139–150.

[26] H. Yamauchi, K. Katayama, A. Yasoshima, K. Uetsuka, H. Nakayama, K. Doi, 1-β-D-Arabinofuranosylcytosine (Ara-C)-induce apoptosis in the rat fetal tissues and placenta, J Toxicol Pathol 16 (2003) 223–229.

[27] A.U. Zaidi, C. D'Sa-Eipper, J. Brenner, K. Kuida, T.S. Zheng, R.A. Flavell, P. Rakic, K.A. Roth, Bcl-X(L)-caspase-9 interactions in the developing nervous system: evidence for multiple death pathways, J Neurosci 21 (2001) 169–175.

BIOLOGY OF REPRODUCTION 70, 1762–1767 (2004)
Published online before print 6 February 2004.
DOI 10.1095/biolreprod.103.026252

Involvement of p53 in 1-β-D-Arabinofuranosylcytosine-Induced Trophoblastic Cell Apoptosis and Impaired Proliferation in Rat Placenta

Hirofumi Yamauchi,[1] Kei-ichi Katayama, Masaki Ueno, Koji Uetsuka, Hiroyuki Nakayama, and Kunio Doi

Department of Veterinary Pathology, Graduate School of Agricultural and Life Sciences, The University of Tokyo, Tokyo 113-8657, Japan

ABSTRACT

1-β-D-Arabinofuranosylcytosine (Ara-C), a DNA-damaging agent, severely inhibits fetal growth and has teratogenicity. Recently, we reported that Ara-C also causes placental growth retardation and increases placental apoptosis. The aim of the present study is to elucidate the mechanisms of placental injury induced by genotoxic stress and involvement of p53, which mediates apoptosis and cell-cycle arrest after DNA damage. We injected Ara-C into pregnant rats on Day 13 of gestation and examined the placentas from 1 to 48 h after the administration. Terminal deoxynucleotidyltransferase-mediated dUTP end-labeling (TUNEL) revealed that the apoptosis of trophoblastic cells in the placental labyrinth zone increased from 3 h after the treatment and peaked at 6 h before returning to control levels at 48 h. An increase in cleaved caspase-3 immunoreactivity was also detected at 6 h. Proliferative activity as measured by immunohistochemistry for topoisomerase IIα and by mitotic index significantly decreased after the treatment in the labyrinth zone. Immunoreactivity for p53 protein in the placental labyrinth zone was remarkably enhanced and peaked at 3 h after treatment, although no increase in *p53* mRNA expression was detected with a reverse transcription-polymerase chain reaction. Regarding p53 target genes, *p21*, *cyclinG1*, and *fas* mRNA levels increased significantly and peaked at around 9 h after the treatment. These results indicate that Ara-C would induce apoptosis and impair cell proliferation in the placental labyrinth zone, and p53 and its transcriptional target genes may play an important role in the pathogenesis of the Ara-C-induced placental toxicity.

apoptosis, conceptus, placenta, toxicology, trophoblast

INTRODUCTION

Adequate placental growth and development are crucial to the development of the fetus, and dysfunctions of the placenta may be closely related to fetal developmental disabilities [1]. In the placenta during normal pregnancy in humans and experimental animals, apoptosis is observed in various kinds of component cells and is thought to play physiological roles in placental growth, turnover, and parturition [2–5]. In contrast, increased apoptosis is reported in human placenta complicated with intrauterine growth retardation or other abnormal pregnancies [6–10]. In experimental animals, placental apoptosis is induced concomitant with developmental disabilities such as fetal growth retardation, preterm delivery, and increased resorptions by the administration of N^G-nitro-L arginine methyl ester [11], lipopolysaccharides [12], and glucocorticoids [5] to dams. Thus, the placenta is thought to be susceptible to endocrinological abnormality, inflammatory cytokines, and oxidative stress, and increased placental apoptosis may cause placental dysfunction, resulting in abnormal fetal development.

Embryos and fetuses are vulnerable to genotoxic stress such as DNA damaging agents or radiation, and congenital anomalies are easily induced [13–16]. Genotoxic stress induces apoptosis and cell-cycle arrest in fetal tissues in a p53-dependent way, and this is recognized as a cause of congenital anomalies [15, 17–19]. The *p53*, a tumor suppressor gene, is involved in the regulation of apoptosis and cell-cycle arrest after DNA damage mainly through the transcriptional activation of its target genes, thereby preventing the propagation of damaged cells in a number of different paradigms [20].

However, little attention has been given to the effect of genotoxic stress on the placenta. Recently, ethylnitrosourea, a teratogenic DNA alkylating agent, was reported to induce apoptosis and growth arrest in trophoblastic cells in the placental labyrinth zone with the up-regulation of p53 protein in vivo [21]. 1-β-D-Arabinofuranosylcytosine (Ara-C), a cytidine analogue, is also known as a DNA-damaging agent. Ara-C is used in the clinical treatment for myelogenous leukemia and is associated with fetal growth restrictions and malformations such as microtis, auditory canal atresia, digit anomalies, and lower limb defects in humans [22–24]. It has a teratogenic effect and causes fetal growth retardation also in experimental animals [13, 25, 26]. Previously, we demonstrated that the administration of Ara-C to pregnant rats caused significant decreases of placental weight and thickness of the labyrinth zone with a marked increase in the number of apoptotic cells among trophoblastic cells of the placental labyrinth zone and confirmed that fetal weight was also restricted at 48 h after the administration [27].

The aim of the present study was to investigate the toxic effect of Ara-C in detail and to explore the mechanisms of increased apoptosis and growth inhibition in the placental labyrinth zone. For this purpose, we injected Ara-C into pregnant rats and investigated the sequential changes in the incidence of apoptotic cell death and kinetics of proliferative activity in the placental labyrinth zone histopathologically. In addition, to clarify the involvement of p53 in Ara-C-induced placental toxicity, we examined the sequential expression patterns of p53 protein and the mRNA of *p53* and its transcriptional target genes.

[1]Correspondence: Hirofumi Yamauchi, Department of Veterinary Pathology, Graduate School of Agricultural and Life Sciences, The University of Tokyo, 1-1-1 Yayoi, Bunkyo-ku, 113-8657 Tokyo, Japan.
FAX: 81 3 5841 8185; e-mail: yamauchi-h@umin.ac.jp

Received: 5 December 2003.
First decision: 29 December 2003.
Accepted: 3 February 2004.

ISSN: 0006-3363. http://www.biolreprod.org

TABLE 1. Primer sequences, cycle numbers, and accession numbers.

Gene	Sense primer	Antisense primer	Cycle number	Accession number
p53	ATATGAGCATCGAGCTCCCTCT	CACAACTGCACAGGGCATGT	29	X13058
p21	AAGTATGCCGTCGTCTGTTCG	GGCACTTCAGGGCTTTCTCTT	28	L41275
cyclinG1	GTGTCGGACTGAGCTGCTTTT	TTGGGAGGTGGGTTATCCTGT	25	X70871
fas	AAGAGGAGCGTTCGTGAAACC	GATCAGCAGCCAAAGGAGCTTA	31	D26112
GAPDH	GCTTCACCACCTTCTTGATGTC	GAGTATGTCGTGGAGTCTACTG	21	AF106860

MATERIALS AND METHODS

Animals and Chemicals

Pregnant Slc:Wistar rats (plug day: Day 0 of gestation) were obtained from Japan SLC Inc. (Shizuoka, Japan). They were kept under controlled conditions (temperature, 23 ± 2°C; relative humidity, 55% ± 5%) using an isolator caging system (Niki Shoji Co., Tokyo, Japan) and were fed commercial pellets (MF, Oriental Yeast Co., Tokyo, Japan) and water ad libitum. Ara-C (Sigma, St. Louis, MO) was dissolved in PBS and its concentration was adjusted to 50 mg/ml. The protocol of the present study was approved by the Animal Care and Use Committee of the Graduate School of Agricultural and Life Sciences, The University of Tokyo.

Treatments

Pregnant rats were injected intraperitoneally (i.p.) with 250 mg/kg of Ara-C on Day 13 of gestation (GD13). Under the conditions of this experiment, congenital anomalies and growth retardation were detected at a high rate in perinatal fetuses, although the incidence of fetal death was not markedly increased [25, 26]. At 1, 3, 6, 9, 12, 24, and 48 h after the treatment, six dams each were killed by heart puncture under ether anesthesia, and the placentas were collected. As controls, six pregnant rats were injected i.p. with an equivalent volume of PBS on GD13 and killed at the same time point as Ara-C-treated groups. Of the six dams obtained at each time point, three were used for histopathological analyses and three for reverse transcription-polymerase chain reaction (RT-PCR) analysis.

For the histopathological analysis, collected placentas were fixed in 10% neutral-buffered formalin, and 4-μm paraffin sections were stained with hematoxylin-eosin (HE). The sections were also subjected to the detection of fragmented DNA and immunohistochemical staining.

Detection of Fragmented DNA

Cells with fragmented DNA were detected by the terminal deoxynucleotidyltransferase-mediated dUTP end labeling (TUNEL) method, which was first proposed by Gavrieli [28] and is now widely used for the detection of apoptotic cells, using an apoptosis detection kit (Apop Tag; Intergen, Purchase, NY). In brief, multiple fragmented DNA 3′-OH ends on the section were labeled with digoxigenin-dUTP in the presence of terminal deoxynucleotidyl transferase (TdT). Peroxidase-conjugated anti-digoxigenin antibody was then reacted with the sections. The positive signals were visualized using a peroxidase-diaminobenzidine (DAB) reaction. The sections were then counterstained with methylgreen.

Immunohistochemical Staining

Immunohistochemical staining for cleaved caspase-3, topoisomerase IIα (TIIα), and p53 was carried out on paraffin sections. Cleaved caspase-3 is one of the key executioners of apoptosis and is responsible for the proteolytic cleavage of many key proteins to yield the apoptotic phenotype [29]. TIIα is a proliferation marker of rat and human tissues that is detected in the S to G2/M phase of the cell cycle [30]. Rabbit anticleaved caspase-3 polyclonal antibody (Cell Signaling Technology, Beverly, MA), mouse anti-TIIα monoclonal antibody (DAKO, Carpinteria, CA), and rabbit anti-p53 polyclonal antibody (Santa Cruz Biotechnology, Santa Cruz, CA) were used as primary antibodies. Sections were stained by the labeled streptavidin-biotin (LSAB) method with streptavidin (DAKO) for cleaved caspase-3 and TIIα, and by EnVision+ polymer reagent (DAKO) for p53. The positive signals were visualized with a peroxidase-DAB reaction and then the sections were counterstained with methylgreen.

Morphometry

To examine the incidence of apoptotic cell death, TUNEL-positive trophoblastic cells in the placental labyrinth zone were counted in three randomly chosen placentas from a dam. Three hundred cells were counted in randomly chosen fields of labyrinth zone in each placenta under a light microscope. For the assessment of proliferative activity, TIIα-positive trophoblastic cells were counted on the immunohistochemically stained sections and mitotic cells on the HE-stained sections in the same way. To examine p53 protein expression, p53-positive trophoblastic cells were also counted on the immunohistochemically stained sections. The apoptotic, mitotic, and TIIα- or p53-labeling indices (%) were expressed as the mean ± standard deviation (SD) for 3 dams, and statistical analysis was carried out with Student *t*-test.

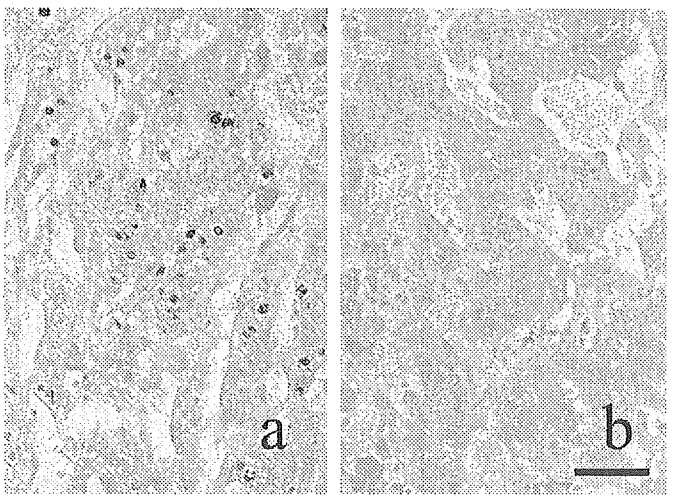

FIG. 1. Placenta of the Ara-C-treated (**a**) and control (**b**) rats at 6 h after the treatment. Many TUNEL-positive trophoblastic cells are seen in the labyrinth zone in **a**. TUNEL staining; bar = 55 μm.

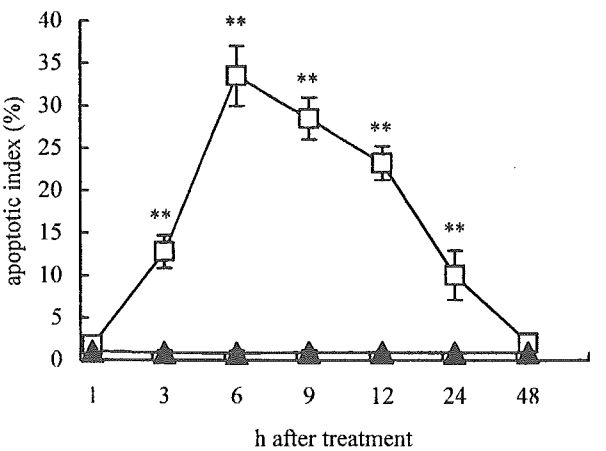

FIG. 2. Apoptotic index in the labyrinth zone. The number of apoptotic trophoblastic cells peaked at 6 h and returned to control levels at 48 h after the treatment. Data represent the mean ± SD (n = 3). **, $P < 0.01$; significantly different from controls. Open squares, Ara-C-treated group; closed triangles, control group.

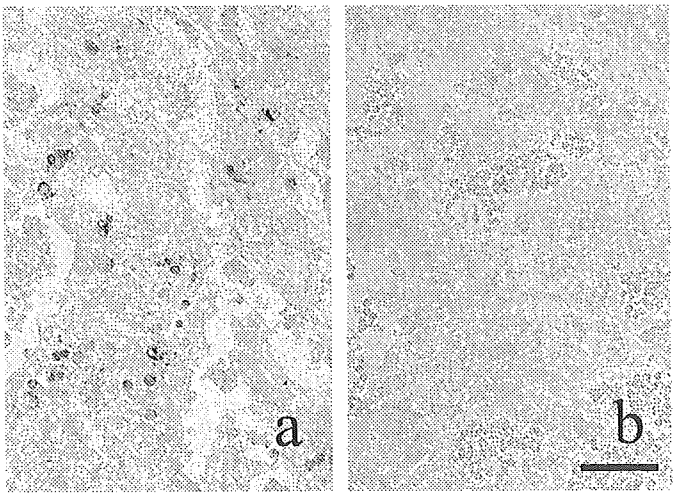

FIG. 3. Placenta of the Ara-C-treated (**a**) and control (**b**) rats at 6 h after the treatment. Many positive signals for cleaved caspase-3 are detected in the trophoblastic cells of the labyrinth zone in **a**. Immunostaining for cleaved caspase-3; bar = 40 μm.

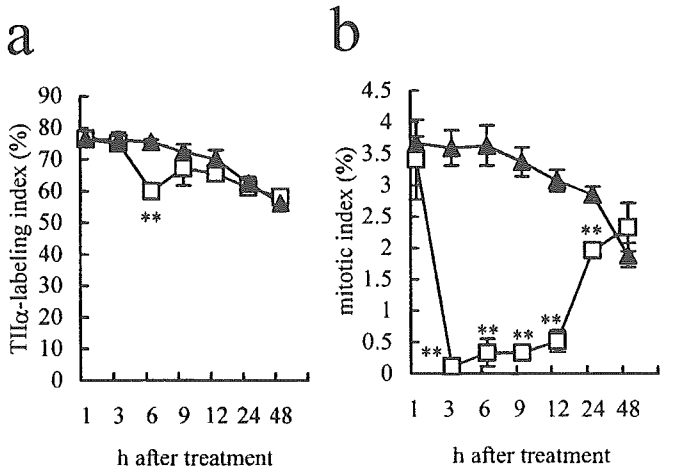

FIG. 5. TIIα-labeling (**a**) and mitotic (**b**) indices in the labyrinth zone. A significant decrease in the immunoreactivity for TIIα was detected at 6 h after the Ara-C-treatment. The number of mitotic figures was significantly suppressed from 3 to 24 h after the treatment. Data represent the mean ± SD (n = 3). **, $P < 0.01$; significantly different from controls. Open squares, Ara-C-treated group; closed triangles, control group.

RNA Extraction and Semiquantitative RT-PCR

The mRNA expression of p53 and three of its well-known target genes, *p21* [31], *cyclinG1* [32], and *fas* [33], was examined. Protein p21 is an inhibitor of cyclin-dependent kinases and induces cell-cycle arrest at the G1 phase [34]. CyclinG1 dephosphorylates mdm2, a negative regulator of p53, and modulates its function [35]. Fas is a type I membrane protein that belongs to the tumor necrosis factor receptor/nerve growth factor receptor family, and it induces apoptosis when it binds to fas ligand [36].

Three or four randomly chosen placentas from a dam were dissected to remove decidua and pooled. Then total RNA was extracted using Isogen (Nippon Gene Co. Ltd., Toyama, Japan). The reverse transcriptase reaction for synthesis of the first strand cDNA was carried out with 15 μg of sample in 60 μl of reaction mixture using oligo$(dT)_{12-18}$ primer and a SUPERSCRIPT Preamplification System (Invitrogen, Carlsbad, CA). PCR was performed with pairs of oligonucleotide primers corresponding to the cDNA sequences of the rat mRNA (Table 1). PCR was carried out with 1 μl of RT product in a 100-μl reaction mixture containing 50 pM of sense and antisense primer, 1.25 U of rTaq, 10× PCR buffer and dNTP mixture (Takara, Ohtsu, Japan). This was immediately followed by preheating at 94°C for 7 min, denaturation at 94°C for 1 min, annealing at 58.5°C for 1 min, and extension at 72°C for 1 min using a Takara PCR Thermal Cycler MP (Takara). Cycle numbers for different reactions are shown in Table 1. Optimal cycle numbers were determined in a preliminary experiment to ensure that the amplification of each gene was in the linear range and not during the plateau phase. PCR products were identified by electrophoresis on 2% agarose gels (Nippon Gene Co. Ltd.) followed by ethidium bromide (Invitrogen) staining. Fluorescent-gel imaging was carried out using an ultraviolet-CCD video system Fas-III (Toyobo, Tokyo, Japan). The results are shown relative to glyceraldehyde-3-phosphate dehydrogenase (GAPDH) expression. The relative band density is presented as the mean ± SD for three dams and statistical analysis was carried out using Student *t*-test.

RESULTS

Incidence of Apoptosis

From 3 h after the Ara-C treatment, the number of TUNEL-positive nuclei, which showed pyknosis on HE-stained sections, began to increase in trophoblastic cells of the placental labyrinth zone (Fig. 1). In our previous study, it was confirmed that the ultrastructural characteristics of these pyknotic cells were consistent with those of apoptotic

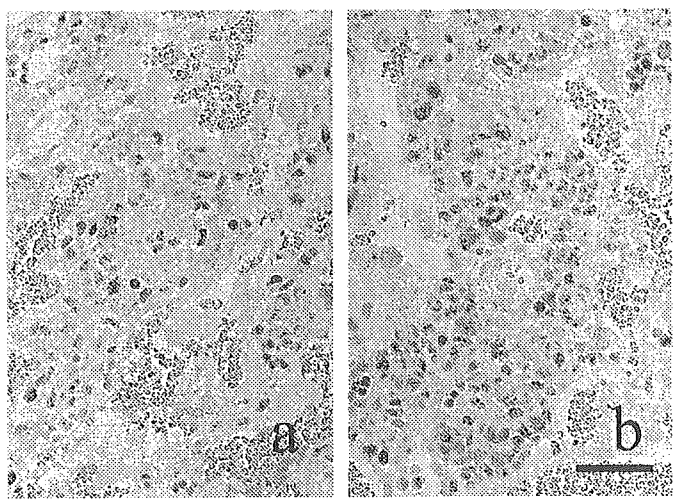

FIG. 4. Placenta of the Ara-C-treated (**a**) and control (**b**) rats at 6 h after the treatment. The number of TIIα-positive nuclei of trophoblastic cells is decreased in the labyrinth zone in **a**. Immunostaining for TIIα; bar = 55 μm.

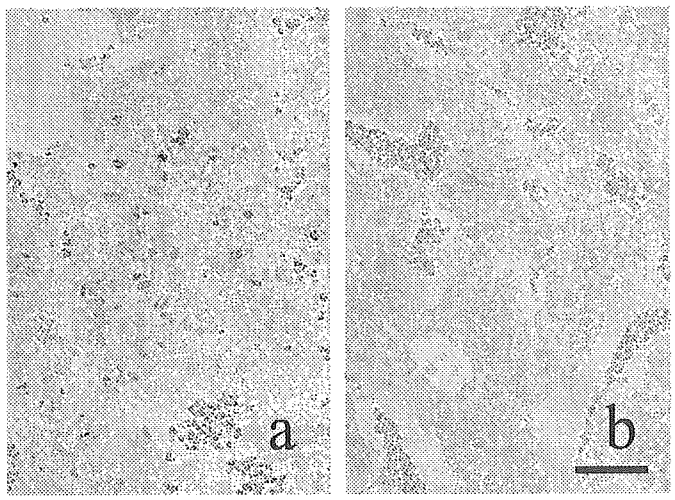

FIG. 6. Placenta of the Ara-C-treated (**a**) and control (**b**) rats at 3 h after the treatment. Many positive signals for p53 are detected in the nuclei of trophoblastic cells in the labyrinth zone in **a**. Immunostaining for p53; bar = 55 μm.

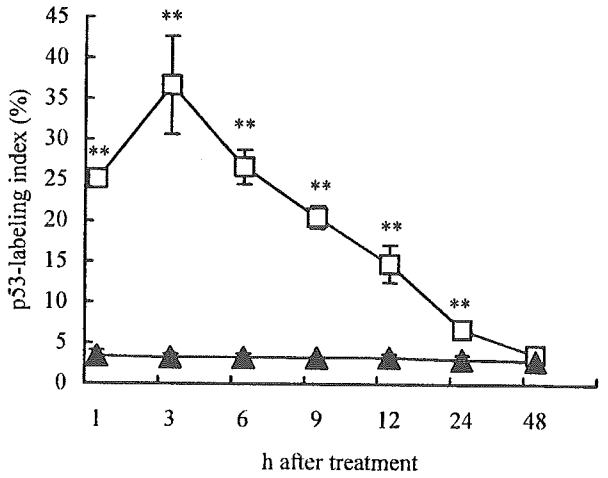

FIG. 7. The p53-labeling index in the labyrinth zone. The number of p53-positive nuclei of trophoblastic cells peaked at 3 h and returned to control levels at 48 h after the treatment. Data represent the mean ± SD (n = 3). **, $P < 0.01$; significantly different from controls. Open squares, Ara-C-treated group; closed triangles, control group.

cells [27]. The number peaked at 6 h after the treatment and returned to control levels at 48 h (Fig. 2). Only a few apoptotic cells were observed in the placental labyrinth zone in control dams throughout the experimental period (Figs. 1 and 2). In the placental basal zone of both the Ara-C-treated and control dams, only a few pyknotic cells were detected (data not shown).

At 6 h after the Ara-C-treatment, many positive signals for cleaved caspase-3 were detected in the trophoblastic cells of the placental labyrinth zone by immunohistochemistry (Fig. 3). On the other hand, only a few positive signals were observed in the placental labyrinth zone of control dams at 6 h after the treatment (Fig. 3).

Proliferative Activity

With the immunohistochemistry for TIIα, many positive signals were observed in the trophoblastic cells of the placental labyrinth zone in both the Ara-C-treated and control groups. A significant decrease in the immunoreactivity was detected at 6 h after the treatment (Figs. 4 and 5). The number of mitotic figures in the placental labyrinth zone decreased rapidly and reached a minimum at 3 h after the Ara-C treatment. The mitotic index was suppressed significantly until 24 h after the treatment, and then returned to control levels at 48 h (Fig. 5).

Expression of p53 Protein

In the placental labyrinth zone of the Ara-C-treated group, the number of p53-positive signals in the nuclei of trophoblastic cells began to increase from 1 h and peaked at 3 h after the treatment (Fig. 6). Then the number declined from 6 h and returned to control levels at 48 h after the treatment (Fig. 7). In the control group, only a few p53-positive signals were observed in the labyrinth zone throughout the experimental period (Figs. 6 and 7).

Expression of p53 and Its Transcriptional Target Genes mRNAs

The expression of *p53* mRNA changed little throughout the experimental period. The expression of *p21, cyclinG1,* and *fas* mRNAs significantly increased in the Ara-C-treated group. The expression of *p21, cyclinG1,* and *fas* mRNAs gradually increased from 3 h and peaked at around 9 h, then returned to control levels at 24 or 48 h after the treatment (Figs. 8 and 9).

DISCUSSION

As mentioned above, we previously demonstrated that the administration of Ara-C to pregnant rats caused significant decreases of placental weight and thickness of the labyrinth zone concomitant with increased apoptosis in the trophoblastic cells of the placental labyrinth zone [27]. In the present study, we detected a marked increase in the number of TUNEL-positive cells from 3 h to 24 h after the exposure to Ara-C. We also observed increased immunoreactivity for cleaved caspase-3. Caspase-3 is an effector of apoptosis thought to have a tissue- and stimulus-specific function [29]. We considered that caspase-3 would be an important executor of apoptosis also in placenta exposed to genotoxic stress. In addition, an analysis of TIIα-labeling and mitotic indices showed that proliferative activity was substantially suppressed in trophoblastic cells of the placental labyrinth zone. These results suggest that both increased cell death and suppressed cell proliferation result in the growth inhibition of the placenta observed in our previous report.

Several investigators recently demonstrated that, strictly speaking, the TUNEL technique is not specific for apoptosis and it also detects a small population of necrotic cells [37]. However, in our studies, TUNEL-positive trophoblastic cells were considered to be apoptotic ones judging from their electron microscopical features [27] and immunoreactivity for cleaved caspase-3.

Increased apoptosis is reported in human placenta complicated with intrauterine growth retardation or other abnormal pregnancies, and it is believed to be associated with placental dysfunction [6–10]. Trophoblastic cells in the placental labyrinth zone are a barrier to transport between maternal and fetal blood that actively facilitate the feto-maternal exchange of nutrients such as glucose, amino acids, fatty acids, and nucleosides [38]. Thus, a functional placental labyrinth zone would be indispensable for the

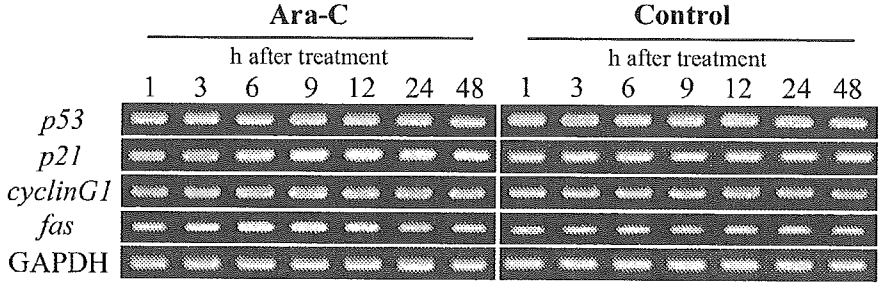

FIG. 8. Sequential changes in the mRNA expression of *p53* and its target genes. The expression of p53 target genes is enhanced after the Ara-C treatment. Agarose gel electrophoresis.